

MgGa₂O₄ spinel barrier for magnetic tunnel junctions: coherent tunneling and low barrier height

Hiroaki Sukegawa,^{1,*} Yushi Kato,² Mohamed Belmoubarik,¹ P.-H. Cheng,^{1,3} Tadaomi Daibou,² Naoharu Shimomura,² Yuuzo Kamiguchi,² Junichi Ito,² Hiroaki Yoda,² Tadakatsu Ohkubo,¹ Seiji Mitani,^{1,3} Kazuhiro Hono^{1,3}

¹*Research Center for Magnetic and Spintronic Materials, National Institute for Materials Science (NIMS), 1-2-1 Sengen, Tsukuba 305-0047, Japan*

²*Corporate Research & Development Center, Toshiba Corporation 1, Komukai-Toshiba-Cho, Saiwai-ku, Kawasaki 212-8582, Japan*

³*Graduate School of Pure and Applied Sciences, University of Tsukuba, Tsukuba 305-8577, Japan*

Abstract

Epitaxial Fe/magnesium gallium spinel oxide (MgGa₂O₄)/Fe(001) magnetic tunnel junctions (MTJs) were fabricated by magnetron sputtering. Tunnel magnetoresistance (TMR) ratio up to 121% at room temperature (196% at 4 K) was observed, suggesting a TMR enhancement by the coherent tunneling effect in the MgGa₂O₄ barrier. The MgGa₂O₄ layer had a spinel structure and it showed good lattice matching with the Fe layers owing to slight tetragonal lattice distortion of MgGa₂O₄. Barrier thickness dependence of the tunneling resistance and current-voltage characteristics revealed that the barrier height of the MgGa₂O₄ barrier is much lower than that in an MgAl₂O₄ barrier. This study demonstrates the potential of Ga-based spinel oxides for MTJ barriers having a large TMR ratio at a low resistance area product.

* Electronic mail: sukegawa.hiroaki@nims.go.jp

Magnetic tunnel junctions (MTJs) have played a central role in spintronic devices such as read heads of hard disk drives and non-volatile magnetoresistive random access memories (MRAMs) for the last two decades, and many efforts have been made to improve their performance.¹ One of the most prominent achievements which accelerated the practical applications was the realization of giant tunnel magnetoresistance (TMR) ratios by using rock-salt type MgO crystalline barrier.²⁻⁵ The giant TMR effect is attributed to the spin-dependent coherent tunneling through the Δ_1 Bloch state in MgO(001). Toward ultra-high density spin transfer torque (STT)-MRAM applications, MTJs with low resistance area (RA) product of around $1 \Omega \cdot \mu\text{m}^2$ are needed as well as high TMR ratios. In MgO-based MTJs, the thickness of the MgO barrier must be reduced to a few monoatomic layers for achieving such a low RA , which causes substantial reduction of TMR ratios. This means the necessity of alternative barriers having a low barrier height. Doping other elements into MgO has been known to reduce the MgO barrier height; e.g., Zn^{6,7} and Ti⁸ dopings were reported to provide lower RA values although such dopings are likely to cause reduction of TMR ratios.

Spinel oxide $\text{MgAl}_2\text{O}_4(001)$ barrier also exhibits the coherent tunneling effect,^{9,10} and over 300% TMR ratios at room temperature (RT) were reported in MgAl_2O_4 -based MTJs.^{11,12} Very recently, a TMR ratio at RT of 92% in an MgO/spinel-type $\gamma\text{-Ga}_2\text{O}_3(001)$ bilayer barrier MTJ¹³ and that of 120% in a Li-Mg-Al-O quaternary spinel-based barrier MTJ were reported,¹⁴ showing the capability of the spinel based barriers for MTJs. The lattice spacing of MgAl_2O_4 is 4% smaller than that of MgO. In

addition, the lattice spacing can further be tuned by the Mg/Al composition, leading to the highly lattice-matched interfaces with various ferromagnetic materials.^{9,12} On the other hand, the experimental band gap of MgAl_2O_4 is reported to be 7.8 eV,¹⁵ which is similar to that of MgO (7.58–7.8 eV);¹⁵ therefore, no reduction in RA values using an MgAl_2O_4 barrier was observed.¹⁶ Some of spinel oxides other than MgAl_2O_4 , such as ZnAl_2O_4 , SiMg_2O_4 and SiZn_2O_4 , were predicted to exhibit the similar coherent tunneling effect.¹⁷ It also was suggested that one can tune the band gap by carefully selecting constituent cations of spinel oxides.

MgGa_2O_4 is known as a wide bandgap transparent semiconducting oxide.¹⁸ The lattice constant of MgGa_2O_4 is 0.8280 nm,¹⁹ which is slightly lower than that of MgO with a doubled unit cell (0.842 nm). Therefore, a good lattice matching with FeCo is expected when all the layers are grown with the (001) orientation. Importantly, the reported band gap is 4.9 eV,¹⁸ which is lower than that of MgAl_2O_4 ; consequently, lowering RA values using an MgGa_2O_4 barrier is expected. In this letter, we report the growth of lattice-matched Fe/ MgGa_2O_4 /Fe(001) MTJs using sputtering method. We confirmed that the MgGa_2O_4 layer was epitaxially grown with a spinel structure. A TMR ratio reached 121% at RT (196% at 4 K), indicating the coherent tunneling effect in the MgGa_2O_4 (001) barrier. Moreover, RA values as a function of the barrier thickness and current-voltage characteristics revealed a low barrier height of the MgGa_2O_4 barrier. Therefore, Ga-based spinels are promising as an

alternative MTJ barrier having a low RA value and a high TMR ratio suitable for future spintronic applications.

MTJ stacks were deposited by ultra-high vacuum magnetron sputtering on an MgO single crystalline substrate using the method reported for the Fe/MgAl₂O₄/Fe(001) MTJs.²⁰ The typical stack structure is MgO(001) substrate/Cr (40)/Fe (100)/Mg ($t_{\text{Mg}} = 0$ or 0.6)/MgGa₂O₄ ($t_{\text{MgGa}_2\text{O}_4}$)/Fe (7)/Ir₂₀Mn₈₀ (12)/Ru (10) (unit: nm). For the MgGa₂O₄ layer deposition, RF sputtering of a sintered MgGa₂O₄ target was used. Other metallic layers were deposited by DC sputtering. To obtain a flat film with a high crystallinity, each layer was *in-situ* post-annealed after the deposition at RT. For the MgGa₂O₄ layer, post-annealing temperature of 500°C was used. The Mg layer was inserted to prevent oxidation of the bottom Fe surface during the MgGa₂O₄ growth and post-annealing. After the deposition, the stacks were *ex-situ* annealed at 175°C under a magnetic field of 5 kOe along the Fe[100] direction. The stacks were then patterned into micrometer scale junctions using electron-beam lithography, photolithography, and Ar ion etching. The patterned MTJs were characterized by DC 4 probe method at RT and 4 K. The microstructure of the whole stack was evaluated by high-angle annular dark field scanning transmission electron microscopy (HAADF-STEM) using an FEI Titan G2 80-200 with a probe aberration corrector. The band gap of a sputtered 30-nm-thick MgGa₂O₄ film grown on an MgO(001) substrate was determined to be 4.7 ± 0.1 eV by reflection electron energy loss spectroscopy, which was nearly equivalent to the bulk value of 4.9 eV.¹⁸ Rutherford backscattering

spectrometry (RBS) analysis revealed that the composition of an MgGa_2O_4 thin film was nearly stoichiometric ($\text{Mg}_{16}\text{Ga}_{29}\text{O}_{55}$).

Figure 1 (a) shows the cross-sectional HAADF-STEM image of an $\text{Fe}/\text{MgGa}_2\text{O}_4$ ($t_{\text{MgGa}_2\text{O}_4} = 2$ nm)/Fe structure along the $\text{Fe}[110]$ direction. The image indicates epitaxial growth from the bottom-Fe to the top-Fe layer with (001) orientation and flat MgGa_2O_4 interfaces. No in-plane misfit dislocations were found in the observed area. By averaging in-plane lattices (50 planes) and out-of-plane lattices (total 25 planes) using scale-calibrated HAADF-STEM images, the MgGa_2O_4 lattice was found to be tetragonally distorted; the in-plane (out-of-plane) lattice spacing was determined to be 0.204 nm (0.212 nm). The in-plane spacing of MgGa_2O_4 was equivalent to that of Fe, leading to the lattice-matched interfaces.

Additionally, a nano-beam electron diffraction (NBD) image taken from the area near the MgGa_2O_4 barrier is shown in Fig. 1 (b). The NBD spots from MgGa_2O_4 and Fe reveal the epitaxial relationship of $\text{Fe}(001)[110] \parallel \text{MgGa}_2\text{O}_4(001)[100]$. The $\{022\}$ spots from MgGa_2O_4 indicate the cation-order in the MgGa_2O_4 lattice. This means that the MgGa_2O_4 barrier has a spinel structure with tetragonal distortion although the accurate atomic configuration cannot be determined by analyzing only the present NBD pattern. The lattice constants of the MgGa_2O_4 were calculated to be 0.816 nm (in-plane) and 0.848 nm (out-of-plane). The ground-state structure of MgGa_2O_4 with an inverse spinel structure was predicted to be a tetragonal structure belonging to the space group $P4_322$ (or $P4_122$);²¹

however, the tetragonality in the MgGa_2O_4 layer of this work may be mainly introduced by compressive stress from thick Fe layers under and above the MgGa_2O_4 layer.

In the case of the MgAl_2O_4 barrier with the same post-annealing temperature (500°C), the cation-order was not observed, and thus the MgAl_2O_4 had a halved lattice constant (~ 0.404 nm) of the normal spinel. This suggests that the cation-order occurs in MgGa_2O_4 easier than in MgAl_2O_4 although the difference in the melting point between MgGa_2O_4 (1930°C) and MgAl_2O_4 (2122°C) is small. The tendency of the order-disorder of cation sites can be determined by the constituent elements. In fact, it is reported that behavior of the cation disordering of spinel oxides by ion radiation strongly depends on the constituent elements.^{22,23}

Elemental maps of Mg, Ga, O and Fe in the MTJ using the energy-dispersive X-ray spectroscopy (EDS) are shown in Figs. 1 (c)-(g), which indicate that the barrier layer is chemically homogeneous. Neither segregation nor interdiffusion of each element is observed near the Fe/ MgGa_2O_4 interfaces. Therefore, chemically sharp bottom-Fe/ MgGa_2O_4 and MgGa_2O_4 /top-Fe interfaces were confirmed. The Mg/Ga atomic ratio were estimated to be ~ 0.5 , which is close to the ratio by the RBS analysis for the 30-nm-thick film ($= 0.55$).

Figure 2 shows the TMR ratio as a function of magnetic field for an Fe/Mg ($t_{\text{Mg}} = 0.6$ nm)/ MgGa_2O_4 ($t_{\text{MgGa}_2\text{O}_4} = 3.0$ nm)/Fe MTJ measured at RT and 4 K (bias voltage ~ 5 mV). TMR ratio of 121% was observed at RT (196% at 4 K) in the MTJ, which are much higher than that expected

from the Jullière model ²⁴ (TMR ratio $\sim 40\text{--}50\%$ by assuming an Fe spin polarization of $0.40\text{--}0.45$ ²⁵). Therefore, we conclude that the tunneling spin polarization is significantly enhanced by the MgGa_2O_4 barrier as observed in Fe/MgO/Fe(001) ⁵ and $\text{Fe/MgAl}_2\text{O}_4/\text{Fe(001)}$ MTJs. ^{9,11} This is attributed to the coherent tunneling effect in the $\text{MgGa}_2\text{O}_4(001)$ barrier as predicted in MTJs with spinel oxides. ¹⁷ The observed TMR ratios are comparable to those in the Fe/cation-ordered $\text{MgAl}_2\text{O}_4/\text{Fe(001)}$ MTJ (117% at RT and 165% at 15 K), ⁹ whereas they are much lower than those in Fe/MgO/Fe(001) ($180\text{--}200\%$ at RT) ^{5,26} and Fe/cation-disordered $\text{MgAl}_2\text{O}_4/\text{Fe}$ ($\sim 245\%$ at RT). ²⁰ This could be attributed to the band-folding effect of the Fe Δ_1 bands due to the doubled lattice size of spinel MgGa_2O_4 . ¹⁰ Therefore, the introduction of a cation-disorder into the MgGa_2O_4 barrier or the use of half-metallic ferromagnetic electrodes will be necessary to achieve a much larger TMR ratio in MgGa_2O_4 based MTJs, as examined in the MgAl_2O_4 based ones. ^{11,12}

Lower RA values in the MgGa_2O_4 barrier are expected due to its low barrier height as a consequence of its lower band gap (4.9 eV) ¹⁸ than that of MgAl_2O_4 (7.8 eV) ¹⁵ and that of MgO ($7.58\text{--}7.8\text{ eV}$). ¹⁵ To evaluate the barrier heights, we plotted $\ln(RA)$ of the parallel (P) magnetic configuration at RT as a function of the barrier thickness (t_{barrier}) for $\text{Fe/MgGa}_2\text{O}_4/\text{Fe(001)}$ ($t_{\text{Mg}} = 0\text{ nm}$) and $\text{Fe/MgAl}_2\text{O}_4/\text{Fe(001)}$ MTJs in Fig. 3. To obtain comparable MTJ stacks, we deposited wedge-shaped barriers using direct sputtering and a linear motion shutter for both the barriers. The post-annealing temperature of the barriers was fixed at 500°C . The $\ln(RA)$ for both the cases linearly

increases with t_{barrier} , indicating that direct tunneling is the dominant electron transport mechanism for both the MTJs. As expected, the absolute RA values and the $\ln(RA)$ slope of the MgGa_2O_4 MTJs are much smaller than those of the MgAl_2O_4 MTJs. As a consequence of the smaller $\ln(RA)$ slope of the MgGa_2O_4 MTJs, the RA of the MgGa_2O_4 barrier increases by a factor of 10 with a thickness increment of 0.38 nm, which is much lower than 0.49 nm of the MgAl_2O_4 barrier, as indicated in Fig. 3. These results suggest that MgGa_2O_4 has a lower barrier height than MgAl_2O_4 .

To further examine the barrier height of the MgGa_2O_4 barrier, the current density (J)-bias voltage (V) curves for MTJs with the same barrier thickness were evaluated. Figure 4 (a) shows that the J - V characteristics for parallel (P) and antiparallel (AP) configurations at RT for $\text{Fe}/\text{MgGa}_2\text{O}_4$ (2.4 nm)/Fe ($t_{\text{Mg}} = 0$ nm) and $\text{Fe}/\text{MgAl}_2\text{O}_4$ (2.4 nm)/Fe MTJs. Here, the positive bias corresponds to electron tunneling from the bottom electrode to top one. For both the MTJs, the nearly symmetric curves with respect to the bias direction were observed. Since the RA value of the MgGa_2O_4 barrier is much lower than those of the MgAl_2O_4 one (see Table 1), larger J can be applied to the MgGa_2O_4 -MTJs. In Fig. 4 (b), we replotted the curves for the positive bias with log scales (i.e., $\ln J$ - $\ln V$). In general, the bias voltage where rapid J increase is observed roughly corresponds to the barrier height (unit in eV). Therefore, the MgGa_2O_4 barrier evidently has a lower barrier height than the MgAl_2O_4 barrier consistently with the RA values as discussed earlier. To compare their barrier heights, we also plotted the fitting results in Fig. 4 (b) using the Simmons' equation:²⁷

$$J = (6.2 \times 10^8 / t_{\text{eff}}^2) \{ (\phi_{\text{eff}} - eV/2) \exp[-10.25 t_{\text{eff}} (\phi_{\text{eff}} - eV/2)^{1/2}] - (\phi_{\text{eff}} + eV/2) \exp[-10.25 t_{\text{eff}} (\phi_{\text{eff}} + eV/2)^{1/2}] \}, \quad (1)$$

where J is in A/cm^2 , t_{eff} is the effective barrier thickness in nm, and ϕ_{eff} is the effective barrier height in eV, respectively. Note that in Eq. (1), we did not take into account the effects of asymmetry in the J - V curves⁷ and the image force²⁷ for simplicity. The TMR ratio, RA , and the fitting results were summarized in Table 1. The experimental curves were well fitted by Eq. (1), and both the MTJs are found to have similar t_{eff} values (0.9–1.1 nm) in the P and AP magnetic configurations. On the other hand, the ϕ_{eff} values for the MgGa_2O_4 -MTJ (1.0 eV for P and 1.3 eV for AP) were much lower than that for the MgAl_2O_4 -MTJ (2.1 eV for P and 3.0 eV for AP). Consequently, the Simmons' fit results of the J - V curves also confirm that the low barrier height of the MgGa_2O_4 barrier.

In summary, we demonstrated the growth of lattice-matched epitaxial $\text{Fe}/\text{MgGa}_2\text{O}_4/\text{Fe}(001)$ MTJs. The MgGa_2O_4 barrier has a spinel structure and a tetragonal distortion was observed. The observed TMR ratio up to 121% at RT (196% at 4 K) indicates that the $\text{MgGa}_2\text{O}_4(001)$ barrier shows the coherent tunneling effect. The barrier thickness dependence of RA value and the Simmons' fit of J - V curves suggested a low barrier height of the MgGa_2O_4 barrier compared with that of the MgAl_2O_4 barrier. Therefore, MgGa_2O_4 spinel is a promising MTJ barrier exhibiting a low RA , which is necessary for future high-density MRAM applications. This study shows that spinel oxides give the possibility to tune not only in their lattice constants but also in the in their barrier heights as coherent barriers of MTJs.

This work was partly supported by the ImPACT Program of Council for Science, Technology and Innovation, Japan. P.C. acknowledges National Institute for Materials Science for the provision of a NIMS Junior Research Assistantship.

References

- ¹ H.J.M. Swagten, in *Handbook of Magnetic Materials*, edited by K.H.J. Buschow (Elsevier Science, Amsterdam, 2008), Vol. 17.
- ² W.H. Butler, X.-G. Zhang, T.C. Schulthess, and J.M. MacLaren, *Phys. Rev. B* **63**, 054416 (2001).
- ³ J. Mathon and A. Umersky, *Phys. Rev. B* **63**, 220403(R) (2001).
- ⁴ S.S.P. Parkin, C. Kaiser, A. Panchula, P.M. Rice, B. Hughes, M. Samant, and S.-H. Yang, *Nature Mater.* **3**, 862 (2004).
- ⁵ S. Yuasa, T. Nagahama, A. Fukushima, Y. Suzuki, and K. Ando, *Nature Mater.* **3**, 868 (2004).
- ⁶ Y. Uehara, A. Furuya, K. Sunaga, T. Miyajima, and H. Kanai, *J. Magn. Soc. Jpn.* **34**, 311 (2010).
- ⁷ D.L. Li, Q.L. Ma, S.G. Wang, R.C.C. Ward, T. Hesjedal, X.-G. Zhang, A. Kohn, E. Amsellem, G. Yang, J.L. Liu, J. Jiang, H.X. Wei, and X.F. Han, *Sci. Rep.* **4**, (2014).
- ⁸ Ikhtiar, S. Kasai, P.-H. Cheng, T. Ohkubo, Y.K. Takahashi, T. Furubayashi, and K. Hono, *Appl. Phys. Lett.* **108**, 242416 (2016).
- ⁹ H. Sukegawa, H. Xiu, T. Ohkubo, T. Furubayashi, T. Niizeki, W. Wang, S. Kasai, S. Mitani, K. Inomata, and K. Hono, *Appl. Phys. Lett.* **96**, 212505 (2010).
- ¹⁰ Y. Miura, S. Muramoto, K. Abe, and M. Shirai, *Phys. Rev. B* **86**, 24426 (2012).
- ¹¹ H. Sukegawa, Y. Miura, S. Muramoto, S. Mitani, T. Niizeki, T. Ohkubo, K. Abe, M. Shirai, K. Inomata, and K. Hono, *Phys. Rev. B* **86**, 184401 (2012).
- ¹² T. Scheike, H. Sukegawa, K. Inomata, T. Ohkubo, K. Hono, and S. Mitani, *Appl. Phys. Express* **9**, 53004 (2016).
- ¹³ N. Matsuo, N. Doko, T. Takada, H. Saito, and S. Yuasa, *Phys. Rev. Applied* **6**, 034011 (2016).
- ¹⁴ T. Scheike, H. Sukegawa, and S. Mitani, *Jpn. J. Appl. Phys.* **55**, 110310 (2016).
- ¹⁵ Y.-N. Xu and W.Y. Ching, *Phys. Rev. B* **43**, 4461 (1991).
- ¹⁶ H. Sukegawa, S. Mitani, T. Ohkubo, K. Inomata, and K. Hono, *Appl. Phys. Lett.* **103**, 142409 (2013).
- ¹⁷ J. Zhang, X.-G. Zhang, and X.F. Han, *Appl. Phys. Lett.* **100**, 222401 (2012).
- ¹⁸ Z. Galazka, D. Klimm, K. Irmscher, R. Uecker, M. Pietsch, R. Bertram, M. Naumann, M. Albrecht, A. Kwasniewski, R. Schewski, and M. Bickermann, *Phys. Status Solidi A* **212**, 1455 (2015).
- ¹⁹ R.J. Hill, J.R. Craig, and G.V. Gibbs, *Phys. Chem. Minerals* **4**, 317 (1979).
- ²⁰ M. Belmoubarik, H. Sukegawa, T. Ohkubo, S. Mitani, and K. Hono, *Appl. Phys. Lett.* **108**, 132404 (2016).
- ²¹ A. Seko, K. Yuge, F. Oba, A. Kuwabara, and I. Tanaka, *Phys. Rev. B* **73**, 184117 (2006).
- ²² D. Simeone, C. Dodane-Thiriet, D. Gosset, P. Daniel, and M. Beauvy, *J. Nucl. Mater.* **300**, 151 (2002).
- ²³ G. Baldinozzi, D. Simeone, D. Gosset, S. Surblé, L. Mazérolles, and L. Thomé, *Nucl. Instr. Meth. Phys. Res. B* **266**, 2848 (2008).

- ²⁴ M. Jullière, Phys. Lett. **54A**, 225 (1975).
- ²⁵ R.J. Soulen, Jr., J.M. Byers, M.S. Osofsky, B. Nadgorny, T. Ambrose, S.F. Cheng, P.R. Broussard, C.T. Tanaka, J. Nowak, J.S. Moodera, A. Barry, and J.M.D. Coey, Science **282**, 85 (1998).
- ²⁶ F. Bonell, S. Andrieu, C. Tiusan, F. Montaigne, E. Snoeck, B. Belhadji, L. Calmels, F. Bertran, P. Le Fèvre, and A. Taleb-Ibrahimi, Phys. Rev. B **82**, 92405 (2010).
- ²⁷ J.G. Simmons, J. Appl. Phys. **34**, 1793 (1963).

Figure captions

FIG. 1. (a) HAADF-STEM image of an Fe/MgGa₂O₄ (~2 nm)/Fe multilayer. (b) NBD pattern taken around the MgGa₂O₄ barrier. (c)-(g) EDS elemental maps for (c) STEM image, (d) Mg, (e) Ga, (f) O and (g) Fe.

FIG. 2. TMR curves as a function of magnetic field for an Fe/Mg (0.6 nm)/MgGa₂O₄ (3.0 nm)/Fe MTJ at 4 K and 297 K (RT).

FIG. 3. $\ln(RA)$ for the P state plotted as a function of barrier thicknesses (t_{barrier}) for Fe/MgGa₂O₄/Fe(001) (area: 128 μm^2) and Fe/MgAl₂O₄/Fe(001) MTJs (area: 39 μm^2) measured at RT under a bias voltage below 10 mV. Solid and dotted lines indicate the fitting results using the linear equation: $\ln(RA) = a + b \times t_{\text{barrier}}$, where a and b are fitting parameters. Note that the deviation from the linear fit at the low t_{barrier} region for MgGa₂O₄ is mainly due to the effect of a non-negligible electrode resistance.

FIG. 4. J - V curves of Fe/MgGa₂O₄ or MgAl₂O₄ (2.4 nm)/Fe at RT. (a) J vs. V , and (b) $\ln J$ vs. $\ln V$. In (b), dotted lines show the fitting curves using Eq. (1).

Table

TABLE I. Summary of experimental and fitting results of Fe/barrier/Fe MTJs with 2.4-nm-thick MgGa₂O₄ and MgAl₂O₄ barriers. t_{eff} and ϕ_{eff} are fitting results using Eq. (1).

Barrier/Structure	TMR ratio (%) (at $V = 0$)	Configur- ation	RA ($\Omega \cdot \mu\text{m}^2$) (at $V = 0$)	t_{eff} (nm)	ϕ_{eff} (eV)
MgGa ₂ O ₄ 2.4 nm /Spinel	80	P	3.02×10^3	0.96	1.3
		AP	5.44×10^3	1.1	1.0
MgAl ₂ O ₄ 2.4 nm /Cation-disorder spinel	236	P	1.37×10^5	0.89	3.0
		AP	4.61×10^5	1.1	2.1

Figures

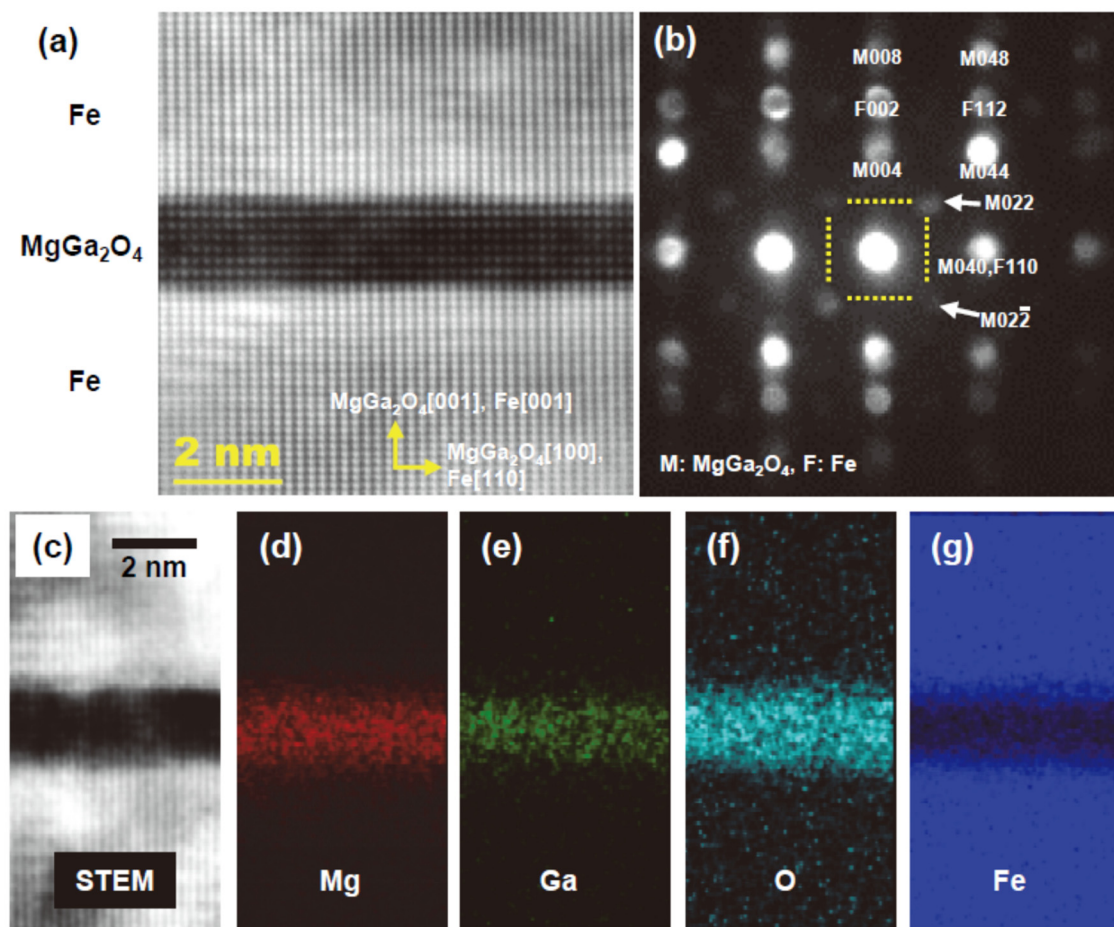


FIG. 1.

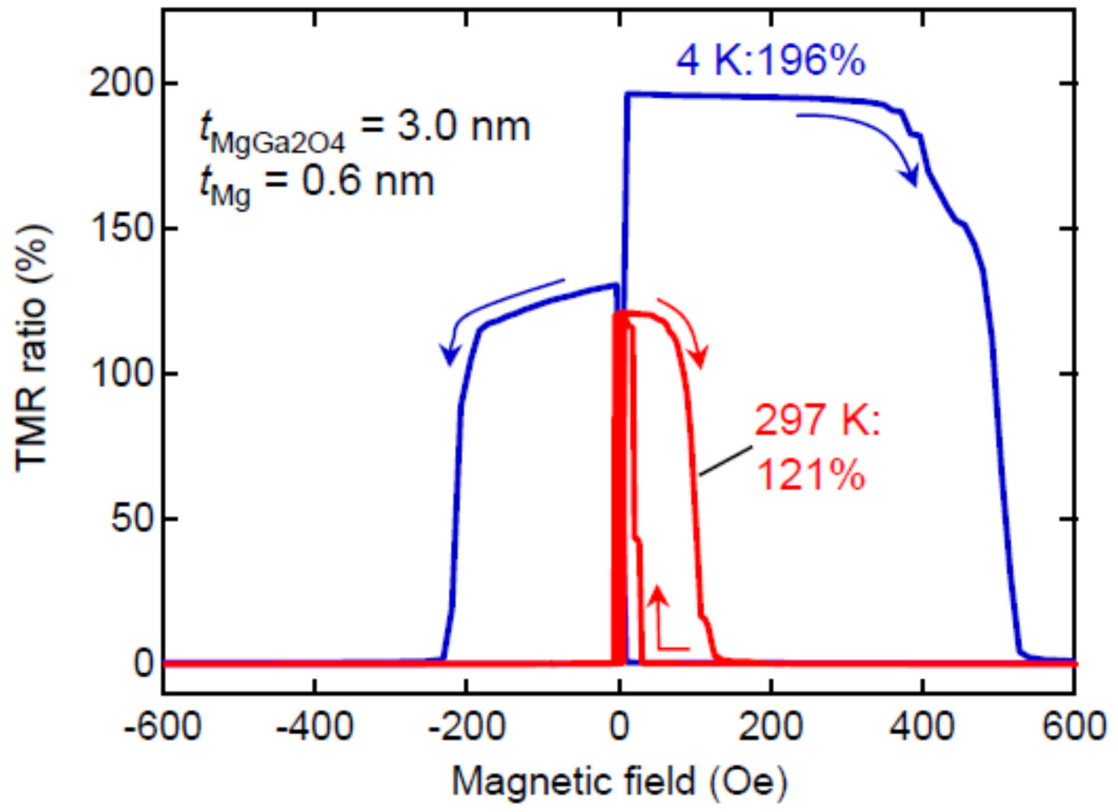


FIG. 2.

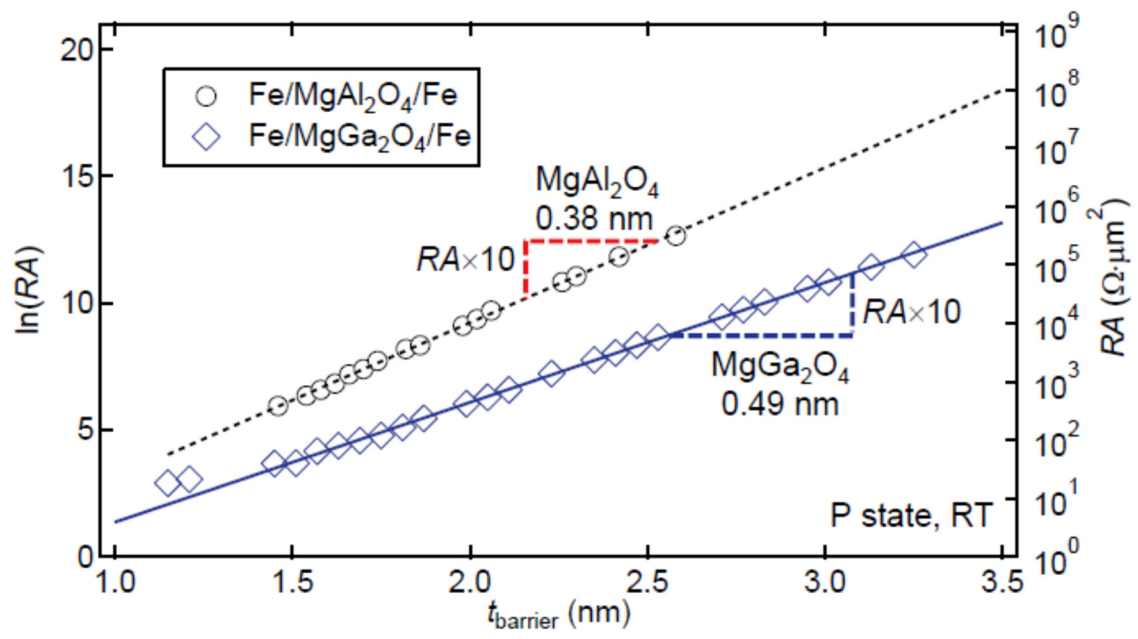


FIG. 3.

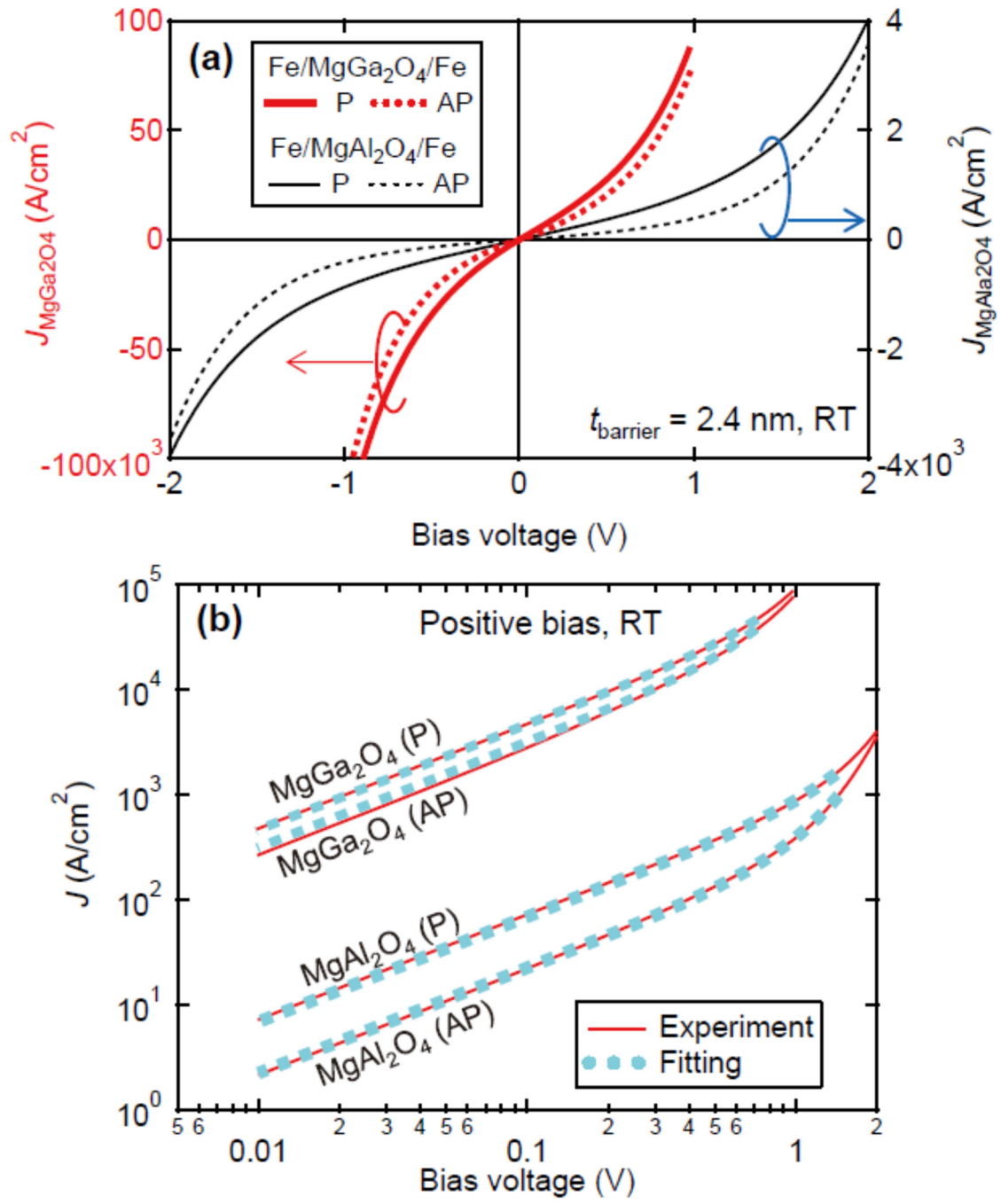


FIG. 4.